Check for updates

# Tuneable emission from disordered to ordered aggregates in substituted 9,10-dihydroanthracene polymers

Erik F. Woering, [ID] †[a] Andrea Taddeucci, [ID] †[b] Andrea Pucci, [ID] *[b] Richard Hildner [ID] *[a] and Marco Carlotti [ID] *[b]

**The fluorescence behaviour of polymers featuring 9,10-dihydroanthracene and oligothiophenyl units was explored under solvent-induced aggregation. Time-resolved spectroscopy using a streak camera and spectral deconvolution revealed multiple aggregate species with distinct characteristics accounting for the unusual emission features observed.**

The development of luminescent materials with adjustable emission colours, particularly in the aggregated or solid state, has attracted great attention due to their potential in optoelectronic devices, fluorescence sensing, bioimaging, and energy technologies.[1,2] Controlling emission in the solid or aggregated state is far more demanding than in dilute solution. In condensed phases, supramolecular interactions and aggregation pathways can radically reshape excited-state dynamics. Here, chemistry plays a decisive role: by tailoring molecular structure and steric environment, one can not only counteract these effects but also exploit them to create entirely new emission behaviours and efficiencies. Aggregation-induced emission (AIE) and its enhanced form (AIEE) have opened broad opportunities for light-emitting materials in the solid state, with applications from optoelectronics to sensing and bioimaging.[3,4] Likewise, thermally activated delayed fluorescence (TADF) has enabled highly efficient photoluminescence in solid-state devices.[5] Together, these concepts have driven major advances in functional organic materials with tuneable aggregate emission, including fluorescent polymers.[6]

Polymers provide highly versatile platforms for structural design. Through careful control of their architecture and composition, they can integrate multiple functionalities, host diverse emitters, and remain solution-processable, making

them powerful matrices for functional fluorescent systems.[7] Although many cases can be explained by the exciton model (H- and J-aggregates), there are also other types of unconventional aggregates, as represented by AIE and AIEE systems.[4] Polymers with fluorescent side-moieties and conjugated polymers are the most representative luminescent polymeric materials[8] and, have been extensively involved in the fabrication of OLED devices, for their intriguingly tuneable optoelectronic properties.[9] Fully conjugated polymers typically show high extinction coefficients and fluorescence properties that are less sensitive to their environment.[10] Yet, research has largely centred on rigid backbones, where strong π–π interactions dictate aggregation pathways. In contrast, semi-flexible backbones that combine conjugated segments with structural "soft spots" remain largely unexplored, despite their unique potential to steer aggregation behaviour and finely tune emissive properties.

In this work, we investigate 9,10-dihydroanthracene (HA)-based conjugated polymers as a platform to study how structural features govern aggregation-driven emission. The sp[3] carbons at the 9 and 10 positions introduce backbone flexibility while maintaining conjugation, allowing steric hindrance and chain packing to be tuned through substituents. By varying both the steric environment and the oligothiophene comonomer length, we reveal how subtle modifications control the balance between single strands, disordered aggregates, and ordered π-stacked species. Using time-resolved streak-camera spectroscopy with spectral deconvolution, we disentangle their emission signatures through decay-associated spectra (DAS) analysis. This approach, applied here for the first time to flexible conjugated polymers, provides new insights into aggregate photophysics and establishes design rules for developing aggregation-sensitive luminescent materials for optoelectronics and sensing.

Unlike common fully conjugated polymers, which are characterized by rigid backbones, the sp[3] carbons in the 9 and 10 positions allow for a more pliant chain (see Fig. S1) without fully suppressing the conjugation.[11] Moreover, the functionalization

[a] Zernike Institute for Advanced Materials, University of Groningen, Nijenborgh 3, 9747 AG, Groningen, The Netherlands. E-mail: r.m.hildner@rug.nl, andrea.pucci@unipi.it

[b] University of Pisa, Dipartimento di Chimica e Chimica Industriale, Via G. Moruzzi 13, 56142, Pisa, Italy. E-mail: marco.carlotti@unipi.it

† These authors contributed to this work equally.

of these positions offers an accessible way to control the steric hindrance around the chain, to suppress strong aggregation, and their chemistry. As a result, HA-containing polymers can be obtained *via* common cross-coupling polymerization protocols, yielding high and controllable degrees of polymerization despite the presence of relatively short solubilizing side groups, as reported in our previous works.[12,13]

The different structures investigated in this work are reported in Fig. 1, together with their absorption and emission profiles. In particular, we employed HA units that displayed on the 9 and 10 positions an identical phenylethynyl group and either a methoxy (OMe) or trimethylsilyloxy (OTMS) moiety to evaluate the influence of the different bulkiness on the aggregation behaviour of the corresponding polymers in solution. Furthermore, we also varied the number of thiophenyl units in the oligothiophenyl comonomer to assess its influence on the resulting optical properties. We observed an evident influence on the *O*-substitution in the fluorescence characteristics, in particular concerning the emission of polymers bearing the OMe side group, which produced intense featureless red-shifted signals (with a Stokes shift > 100 nm) at around 530 nm (Fig. 1). This feature is also present, but much less pronounced, in the corresponding polymers bearing the OTMS group, for which the dominant emission is that of the single-strand species, characterised by smaller Stokes shifts that vary from about 30 nm (in the case of **HA(OTMS)-T**) to about 50 nm (in the case of **HA(OTMS)-TT**). These peculiar features could be ascribed to a suppressed formation of aggregates for OTMS-substituted polymers in solution, whereas aggregate formation seems to be favoured in the case of the less sterically hindered OMe-substituted polymers (especially **HA(OMe)-T**). In agreement with this observation, the absorption spectra of these materials

also show a red-shifted tail, which is more pronounced as the broad 530 nm emission peak gets more intense (Fig. 1). For the OTMS-substituted series, the increasing Stokes shift with the number of thiophenyl units and the structured shape which characterize the emissions, but not the absorption, could be ascribed to excited-state planarization, due to different degrees of torsional flexibility, a common feature observed in conjugated polymers with torsional degrees of freedom.[14–17] It is worth mentioning that in previous studies in which we investigated similar HA polymers characterized by even bulkier groups on the triple bond,[12,13] no aggregate peak was found. This observation suggests that steric hindrance of substituents at the 9 and 10 positions allows to control aggregate formation, to shift the main emission over more than 100 nm, and thus to tune emission colour.

To investigate the aggregation behaviour of these materials, we studied how the emission profiles of the materials changed upon addition of a non-solvent, from pure $CHCl_3$ to $CHCl_3$/MeOH 10 : 90 (Fig. 2 and Fig. S3–S5). To our surprise, in the case of OMe-substituted series, the addition of MeOH caused the progressive disappearance of the band at 530 nm, without initially affecting the most blue-shifted bands we ascribed to single-strand (until up to 70 : 30 $CHCl_3$ : MeOH). Notably, increasing the MeOH concentration further to above 50%vol. a red low-emissive band centred at around 610 nm, was observed for all compounds (Fig. S5). Upon addition of the non-solvent micrometre-sized particles are formed, as confirmed by DLS analysis (Table S1), which suggests that this red emission stems from H-type aggregates. For polymers bearing an OTMS group, the red band that forms upon addition of methanol has a lower wavelength (540 nm, 550 nm, and 570 nm for **HA(OTMS)-T**, **-BT** and **-TT**, respectively).

To understand the emissive species contributing to the spectra in Fig. 2, we investigated how temperature affects the fluorescence. For **HA(OMe)-T** Fig. S8A shows the emission at room temperature with two strong peaks at 530 and 580 nm
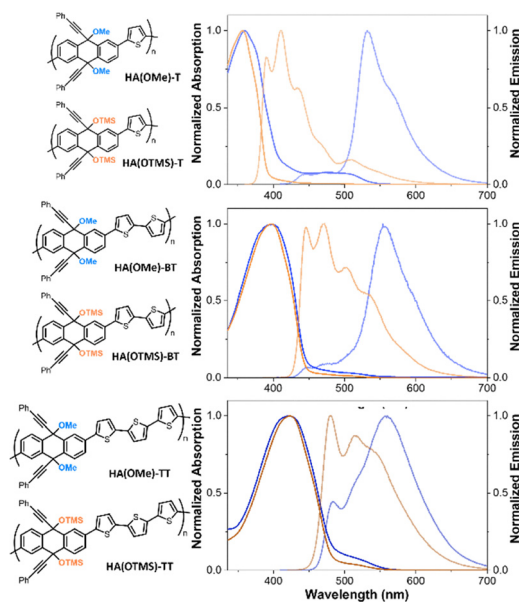


Fig. 1 Molecular structure of the polymers employed in this study and their absorption and emission profiles in $CHCl_3$ (50 µg mL$^{-1}$) at room temperature. Blue and orange spectra refer to OMe- and OTMS-substituted polymers, respectively.
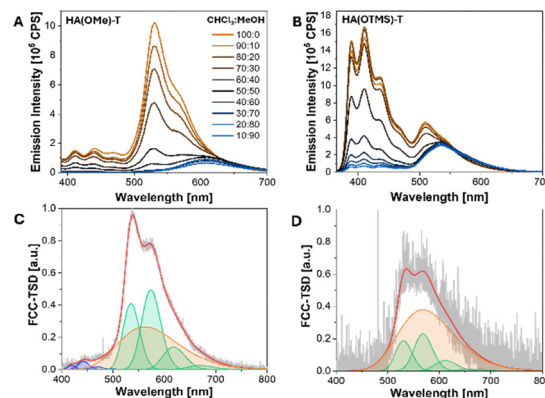


Fig. 2 Fluorescence spectra of **HA(OMe)-T** (A) and **HA(OTMS)-T** (B) in $CHCl_3$ : MeOH mixtures at different compositions (10 µg mL$^{-1}$). For the -BT and -TT polymers see Fig. S3. Temperature-dependent fluorescence spectra of **HA(OMe)-T** in $CHCl_3$ at room temperature (C) and after heating to 60 °C and ambient cooling overnight (D). Each spectrum was fitted using two progressions (blue, green) and a Gaussian function (orange).

and a weak shoulder between 600–700 nm. After heating to 60 °C (Fig. S8B) and after 24 hours of cooling (Fig. S8C), the two main peaks decrease and the shoulder becomes more pronounced, with no detectable emission below 500 nm, indicating changes in the emissive species. For a quantitative analysis of the temperature-dependent spectral changes, we employed Franck–Condon fits (see SI, Section 5) with three components (Fig. 2 and Fig. S8): a weak short-wavelength vibronic progression and, at long wavelengths, a combination of a vibronic progression and a broad Gaussian peak. The Gaussian component represents a structure-less feature emerging at low energy, particularly around 600 nm, and becomes more dominant with temperature. This three-component model fits spectra across all temperatures, with only their relative intensities changing (Fig. S9). An analogous temperature-dependent behaviour was observed for **HA(OTMS)-T** in CHCl$_3$ and in chlorobenzene as control experiment to exclude effects from degradation (Fig. S10).

In order to further investigate the properties of these three components, we performed time-resolved emission measurements on all compounds in chlorobenzene, and for compounds **HA(OMe)-T**, **-BT**, and **-TT** additionally in CHCl$_3$ and in a CHCl$_3$/MeOH (20 : 80) mixture using a streak camera (see SI, Section 1). This technique enables simultaneous detection of spectral and temporal emission features, allowing for disentangling the complex fluorescence dynamics of coexisting emissive species. Fig. 3A and D show the streak-camera measurements for compound **HA(OMe)-T** in CHCl$_3$ and in the mixture, respectively. In the former solvent (Fig. 3A), we observe fluorescence at longer times of 5000 ps (and beyond) for wavelengths above 500 nm, while in the mixture (Fig. 3D) this longer-lived feature is less prominent.

The spectral signatures of the different species are retrieved by extracting decay curves, spectrally integrated over 10 nm intervals across the entire spectral range of the streak data, and fitting each decay curve with a bi-exponential function, which we associate with the decay of different emissive (single-strand and aggregate) species. For the best fit, the lifetimes are constant across the detected spectral range and only the amplitudes of the exponentials are allowed to vary independently.



**Fig. 3** Streak camera data of **HA(OMe)-T** in CHCl$_3$ (A)−(C) and CHCl$_3$/MeOH (20 : 80) (D)−(F). (A) and (D) Streak camera measurements (0.1 μg mL$^{-1}$). (B) and (E) Time traces integrated over the whole spectral range of the streak camera data. The straight lines indicate the decays with a short (cyan) and long lifetime (orange). (C) and (F) Decay associated spectra (DAS) obtained from a global fit of the Streak data, as well as the integrated spectrum of the streak camera (gray).

For **HA(OMe)-T** (Fig. 3) the lifetimes are 250 ps and 2360 ps in CHCl$_3$, and 180 ps and 1600 ps in the mixture. The same analysis was performed on the other polymers obtaining similar findings (see Table S3). Plotting the amplitudes as a function of wavelength decay-associated spectra (DAS) of the species are obtained,[18] which we display in Fig. 3C and F (cyan, orange) together with the total time integrated fluorescence spectra from the streak camera measurements (grey). The time-integrated spectra peak at *ca.* 575 nm closely resemble the steady-state spectra of **HA(OMe)-T** in CHCl$_3$ and in the mixture (see Fig. 2). In both samples, the DAS of the long-lived decay component (orange) are very similar in peak wavelength (∼575 nm), and comparable to the broad (Gaussian) peak around 600 nm in Fig. 2. The long lifetime associated with this DAS (compared to the short-lived DAS associated with single-strand chains, see below) indicates that this species represents H-aggregates formed by ordered π-stacked chains.[19,20] We refer to this species as ordered aggregates in the following. The lifetimes of this long-lifetime DAS vary between polymers and solvents used (see Table S4), which suggests differences in chain packing due to the chemical structure of the backbone and O-substitutions and a difference in radiative rates and fluorescence quantum yields (see SI, section 7 for a more detailed discussion).

The DAS of the short-lived component for **HA(OMe)-T** in CHCl$_3$ and in the mixture (Fig. 3C and F, cyan) are broad and cover the 420–650 nm range. Both DAS have a peak emission around 470 nm with an onset starting at 420 nm and a shoulder at 580 nm, the latter being more pronounced in the case of the mixture. Since these DAS cover the spectral range of the single-strand emission (420–500 nm) and of aggregates (500–650 nm), this indicates that in the range of aggregate emission there is indeed a second species contributing. Moreover, within the time resolution of our setup (∼200 ps), the lifetimes of this second, short-lived aggregate species are very similar to that of the single-strand chains. We therefore attribute this second species to a disordered aggregate. The vibronic progressions of the single-strand and disordered aggregates differ only marginally, *i.e.*, the relative suppression of the 0–0 peak of the latter is only weak (see Table S4) and inter-chain electronic interactions do not substantially change photophysics. Hence, we can expect very similar lifetimes within our time resolution (see also section S7). The more pronounced shoulder in the short-lifetime DAS in the mixture indicates that the relative contribution of disordered aggregates to the total emission is larger in the mixture than in CHCl$_3$, which reduces exposure of the polymer chains with the non-solvent in the mixture. As such, the addition of methanol to the CHCl$_3$ dissolved polymer does not seem to form new aggregates, but rather facilitates the formation of the ordered aggregate. The same behaviour can be seen in the DAS in CHCl$_3$ and the 20 : 80 mix of **HA(OMe)-BT** and **-TT**, as well as the DAS in chlorobenzene for all six polymers (Fig. S9 and S10).

The behaviour and interplay of these different (co-existing) species in solution can be summarised as follows: The signal at short-wavelengths (<500 nm) results from emission of single-strand chains in solution. At long-wavelengths (>500 nm), the combination of the vibronic progression and broad (skewed)
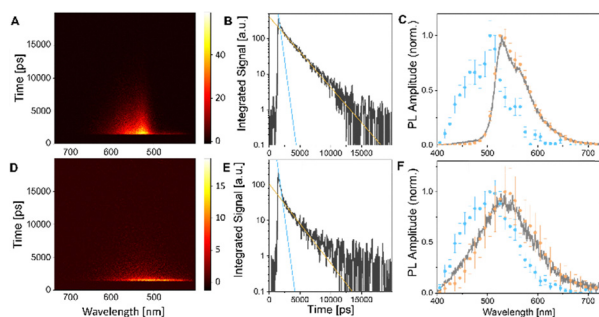
Gaussian peak stems from disordered aggregates and ordered aggregates, respectively. The temperature-dependent data in Fig. S4 indicate that the single-strand chains assemble into ordered aggregates (or attach to ordered aggregates, thus increasing their size, see the DLS data in Table S1). The disordered aggregates transform into ordered aggregates upon heating and cooling (and ageing). As such, the ordered aggregate is presumably a thermo-dynamically stable species, because no single-strand chains are formed by disassembly upon heating to 60 °C, and after cooling down, the spectral profile of the ordered aggregate dominates. We noticed those ordered aggregates for all polymers in chlorobenzene, and for **HA(OMe)-T**, **-BT** and **-TT** in $CHCl_3$, as shown by the presence of the long-lived DAS in the Streak data (see Fig. S11 and S12). The disordered aggregate is probably a kinetically trapped aggregate species that is able to transform into ordered aggregates through a thermally assisted process.

The combination of all these observations allows us to finally comment on the nature of the aggregates. An ordered aggregate is composed of π-stacked chains, in which excitons are delocalised over several neighbouring chains due to inter-molecular electronic interactions.[19,20] This delocalisation results in a distorted vibronic progression in the fluorescence spectra with a suppressed 0-0 peak and increased radiative rates (see section 7, SI). The large variation in aggregate size (Table S1) results in a strong line broadening of the ordered aggregate emission and thus in a skewed Gaussian shape of its fluorescence. In contrast, a disordered aggregate is a small cluster comprising few chains, in which chain segments of neighbouring strands are in (loose) contact to allow for intermolecular interactions, but no defined π-stacking occurs.[21–23] In this situation, excitons remain rather localised on 1-2 neighbouring chain segments due to the large (electronic and structural) disorder.[23,24] Hence, compared to single-strand chains, the fluorescence spectra of such disordered aggregates are very similar in their vibronic progression with only small changes in the relative 0-0 peak signal. The red-shift of the disordered aggregate fluorescence accompanied by the red-shifted tail in the absorption spectra (Fig. 1) results from a change in the local dielectric environment, often referred to as "gas-to-crystal shift", *i.e.*, the solvent surrounding emitting sites in single-strand chains is largely replaced by conjugated segments of other chains surrounding emitting sites in disordered aggregates, a common effect observed for aggregates of conjugated polymers and small molecules.[19,20,24]

Overall, this study highlights how subtle structural variations in 9,10-dihydroanthracene-based polymers, particularly in side-group steric hindrance and conjugation length, profoundly affect aggregation pathways and fluorescence signatures. Through combined time-resolved spectroscopy and spectral deconvolution, we identified and disentangled emission from single strands, disordered aggregates, and long-lived ordered π-stacked species. These insights expand the understanding of emission mechanisms in flexible conjugated polymers and pave the way for the rational design of aggregation-sensitive materials for optoelectronic or sensing applications.

## Conflicts of interest

There are no conflicts to declare.

## Data availability

The data supporting this article have been included in the main article and as part of the supplementary information (SI). Supplementary information is available. See DOI: https://doi.org/10.1039/d5cc04688b.

Raw data are available from the corresponding authors upon reasonable request.

## Notes and references

1 S. Ye and Y. Bao, *Chem. Mater.*, 2024, **36**, 5878–5896.
2 X. Wu and C. Barner-Kowollik, *Chem. Sci.*, 2023, **14**, 12815–12849.
3 X. Cai and B. Liu, *Angew. Chem., Int. Ed.*, 2020, **59**, 9868–9886.
4 S. Ma, S. Du, G. Pan, S. Dai, B. Xu and W. Tian, *Aggregate*, 2021, **2**, e96.
5 S. J. Zou, Y. Shen, F. M. Xie, J. De Chen, Y. Q. Li and J. X. Tang, *Mater. Chem. Front.*, 2020, **4**, 788–820.
6 R. Hu, A. Qin and B. Z. Tang, *Mater. Chem. Front.*, 2020, **4**, 788–820.
7 Y. Bao, *Molecules*, 2021, **26**, 6267.
8 Z. Qiu, B. A. G. Hammer and K. Müllen, *Prog. Polym. Sci.*, 2020, **100**, 101179.
9 T. Wang, Y. Zou, Z. Huang, N. Li, J. Miao and C. Yang, *Angew. Chem., Int. Ed.*, 2022, **61**, e202211172.
10 M. S. Vezie, S. Few, I. Meager, G. Pieridou, B. Dörling, R. S. Ashraf, A. R. Goñi, H. Bronstein, I. McCulloch, S. C. Hayes, M. Campoy-Quiles and J. Nelson, *Nat. Mater.*, 2016, **15**, 746–753.
11 M. Carlotti, A. Kovalchuk, T. Wächter, X. Qiu, M. Zharnikov and R. C. Chiechi, *Nat. Commun.*, 2016, **7**, 13904.
12 B. Bertoncini, A. Taddeucci, S. Trano, S. Raviolo, I. Valdrighi, F. M. Vivaldi, V. Mattoli, F. Bella and M. Carlotti, *Small Methods*, 2025, **9**, 2500488.
13 M. Carlotti, T. Losi, F. De Boni, F. M. Vivaldi, E. Araya-Hermosilla, M. Prato, A. Pucci, M. Caironi and V. Mattoli, *Polym. Chem.*, 2023, **14**, 4465–4473.
14 K. H. Park, W. Kim, J. Yang and D. Kim, *Chem. Soc. Rev.*, 2018, **47**, 4279–4294.
15 S. Tretiak, A. Saxena, R. L. Martin and A. R. Bishop, *Phys. Rev. Lett.*, 2002, **89**, 097402.
16 S. T. Hoffmann, H. Bässler, J.-M. Koenen, M. Förster, U. Scherf, E. Scheler, P. Strohriegl and A. Köhler, *Phys Rev B: Condens Matter Mater. Phys.*, 2010, **81**, 115103.
17 J. Gierschner, J. Shi, B. Milián-Medina, D. Roca-Sanjuán, S. Varghese and S. Park, *Adv. Opt. Mater.*, 2021, **9**, 2002251.
18 I. H. M. van Stokkum, D. S. Larsen and R. van Grondelle, *Biochim. Biophys. Acta, Bioenerg.*, 2004, **1657**, 82–104.
19 N. J. Hestand and F. C. Spano, *Chem. Rev.*, 2018, **118**, 7069–7163.
20 F. C. Spano, *Acc. Chem. Res.*, 2010, **43**, 429–439.
21 Y. Huang, H. Cheng and C. C. Han, *Macromolecules*, 2010, **43**, 10031–10037.
22 Y. Huang, H. Cheng and C. C. Han, *Macromolecules*, 2011, **44**, 5020–5026.
23 D. Raithel, S. Baderschneider, T. B. de Queiroz, R. Lohwasser, J. Köhler, M. Thelakkat, S. Kümmel and R. Hildner, *Macromolecules*, 2016, **49**, 9553–9560.
24 B. Wittmann, F. A. Wenzel, S. Wiesneth, A. T. Haedler, M. Drechsler, K. Kreger, J. Köhler, E. W. Meijer, H.-W. Schmidt and R. Hildner, *J. Am. Chem. Soc.*, 2020, **142**, 8323–8330.